Glycobiology vol. 21 no. 12 pp. 1651–1662, 2011
doi:10.1093/glycob/cwr101
Advance Access publication on August 1, 2011

Is *N*-acetyl-D-glucosamine a rigid $^4C_1$ chair?

Benedict M Sattelle and Andrew Almond[1]

Manchester Interdisciplinary Biocentre, 131 Princess Street, Manchester M1 7DN, UK

Received on June 3, 2011; revised on June 28, 2011; accepted on July 19, 2011

Understanding microsecond-timescale dynamics is crucial to establish three-dimensional (3D) structure–activity relationships in sugars but has been intractable to experiments and simulations. As a consequence, whether arguably the most important chemical scaffold in glycobiology, *N*-acetyl-D-glucosamine (GlcNAc), deviates from a rigid $^4C_1$ chair is unknown. Here, conformer populations and exchange kinetics were quantified from the longest aqueous carbohydrate simulations to date (0.2 ms total) of GlcNAc, four derivatives from heparan sulfate and their methylglycosides. Unmodified GlcNAc took 3–5 μs to reach a conformational equilibrium, which comprised a metastable $^4C_1$ chair that underwent $^4C_1 \leftrightarrow {}^1C_4$ transitions at a predicted forward rate of 0.8 μs^{-1} with an average $^1C_4$-chair lifetime of 3 ns. These predictions agree with high-resolution crystallography and nuclear magnetic resonance but not with the hypothesis that GlcNAc is a rigid $^4C_1$ chair, concluded from previous experimental analyses and non-aqueous modeling. The methylglycoside was calculated to have a slower forward rate (0.3 μs^{-1}) and a more stable $^4C_1$ conformer (0.2 kcal mol^{-1}), suggesting that pivotal 3D intermediates (particularly ^2S_O, $^1S_5$ and $B_{2,5}$) increased in energy, and water was implicated as a major cause. Sulfonation (*N*-, 3-*O* and 6-*O*) significantly augmented this effect by blocking pseudorotation, but did not alter the rotational preferences of hydroxyl or hydroxymethyl groups. We therefore propose that GlcNAc undergoes puckering exchange that is dependent on polymerization and sulfo substituents. Our analyses, and 3D model of the equilibrium GlcNAc conformer in water, can be used as dictionary data and present new opportunities to rationally modify puckering and carbohydrate bioactivity, with diverse applications from improving crop yields to disease amelioration.

Keywords: glucosamine / heparan sulfate / kinetics / pucker / simulation

Introduction

Understanding carbohydrate three-dimensional (3D) structure–activity relationships (SARs) is a difficult but critical milestone in glycomics. Elucidating molecular details of glycan equilibrium 3D structure, presently in its infancy, are central to realizing accurate SARs and will enable rational exploitation of the vast medicinal and industrial potential of polysaccharides. The hexosamine chemical scaffold of *N*-acetyl-D-glucosamine (GlcNAc) is ubiquitous and mediates some of the most important processes in glycobiology. Consequently, establishing SARs in GlcNAc and its derivatives will engender innumerable opportunities to impact some of the most challenging scientific problems of our time. For example, as well as being a versatile scaffold for novel drug discovery (Wang et al. 2009), chemically modified GlcNAc is present in chitin and glycosaminoglycans, which hold great potential as novel biomaterials and medicines (Gama et al. 2006; Murrey and Hsieh-Wilson 2008; Khoushab and Yamabhai 2010).

The 3D structures of GlcNAc polysaccharides are defined by two dynamic conformational determinants: glycosidic linkage geometry and pyranose ring conformation (or pucker). Nanosecond gycosidic-linkage dynamics are better understood because they are amenable to study by both nuclear magnetic resonance (NMR) spectroscopy and simulation. However, while puckering is central to glycobiology, e.g. ribose differs from deoxyribose by having different equilibrium conformations (Rich 2003), whether substituents affect the ensemble of pyranose ring conformers remains enigmatic because exchange occurs on microsecond timescales, which has been problematic for NMR and simulations, until recently (Sattelle et al. 2010).

There is circumstantial experimental evidence to suggest that pyranoses, such as glucose and GlcNAc (considered to exist as exclusively stable $^4C_1$ chairs), are not as stable as once thought. For example, atomic force microscopy has inferred that glucose polymers contain non-$^4C_1$ geometries (Marszalek et al. 1998; Heymann and Grubmuller 1999; Li et al. 1999), and non-$^4C_1$ GlcNAc is observed in high-resolution crystallographic 3D structures of diverse (non-enzyme) protein co-complexes (Ikemizu et al. 1999; Chang et al. 2003; Maveyraud et al. 2009; Xu et al. 2010). Furthermore, studies have also shown that apparently stable $^4C_1$ chairs can be perturbed by chemical modifications, e.g. glucuronic acid (β-D-GlcA) deviates from a $^4C_1$ chair in fully *O*-sulfonated chondroitin and hyaluronan (Wessel and Bartsch 1995; Maruyama et al. 1998; Toida et al. 1999, 2000).

[1]To whom correspondence should be addressed: Tel: +44-161-306-4199; Fax: +44-161-306-5201; e-mail: andrew.almond@manchester.ac.uk

While NMR would be an ideal technique to explore these observations, puckering exchange occurs on the microsecond timescale, which is fast-enough to ensure that standard experiments cannot discriminate between conformers (resonances represent "average" puckers) and interpretation of anything but the simplest situation is difficult. Under ideal conditions, using scalar couplings, the minimum percentage of perceptible conformers is around 10%. Simulations are crucially important in this microsecond "blind spot," but have not been routinely possible with explicit solvent due to lack of processing power (most previous simulations are <100 ns). Recently, implementation of molecular dynamics (MD) programs to run on graphics processing units have made it possible to perform deterministic unperturbed explicit solvent simulations on microsecond timescales (Harvey et al. 2009; Klepeis et al. 2009). Extended molecular mechanics studies are currently restricted to single chemistries but have recently revealed biologically relevant insight into carbohydrate puckering populations and exchange kinetics (Sattelle et al. 2010). Measurements from NMR (e.g. pyranose ring vicinal couplings) can then be usefully applied to test the simulations.

The potential rewards of understanding SARs in GlcNAc-containing polysaccharides are exemplified by heparan sulfate (HS) and structurally related heparin (Powell et al. 2004; Lamanna et al. 2007; Turnbull 2010). Localized in the extracellular matrix, HS mediates of some of the most important processes in biology, e.g. neuronal development (Zhu et al. 2010), anticoagulation (Liu and Pedersen 2007) and angiogenesis (Sasisekharan et al. 2002). In vivo, heterogeneous HS polymers of variable length are bound to proteins via rigid sulfonated (S-)domains (Bishop et al. 2007), which are flanked by flexible unsulfonated (NA-)regions (Mobli et al. 2008). The monosaccharides GlcA and GlcNAc comprise the disaccharide repeat in NA domains, while sulfonated derivatives of α-L-iduronic acid (IdoA) and GlcNAc predominate in S-domains; IdoA can be 2-*O*-sulfonated (IdoA2S) and GlcNAc can be *N*-, *6*-*O*- and *3*-*O*-sulfonated, leading most commonly to GlcNS, GlcNS6S, GlcNS6S3S and GlcNS3S (Figure 1). Anticoagulant heparin is one of the oldest and most widely used natural product drugs; synthetic alternatives are highly desirable due to clinical dangers associated with impure material (Liu et al. 2009). Heparin potency is dependent on the charged carboxyl and sulfo substituents of its uronic acid and hexosamine residues (Hricovini et al. 2001; Avci et al. 2003). Puckering is also a key contributor, the protein antithrombin (ATIII) binds the $^{2}S_{O}$ pucker of the heparin IdoA2S residue (Hricovini et al. 2001) and derivatives exhibiting $^{2}S_{O}$-biased IdoA2S are highly efficacious (Das et al. 2001; Boltje et al. 2009). Exactly how different sulfonation patterns impart functional diversity in HS and heparin remains unclear; however, they are well characterized and therefore provide excellent model systems for chemically modified carbohydrates in general.

In this study, we aim to explore the equilibrium populations and exchange kinetics of GlcNAc puckers and also the effects of sulfo substituents and methylglycosides on them. The most extensive all-atom explicit solvent carbohydrate simulations to date were performed (0.2 ms in total), and experimentally validated, for GlcNAc, GlcNS, GlcNS6S, GlcNS6S3S and GlcNS3S as free α-anomers and methylglycosides. Our findings suggested that in water, despite being a metastable $^{4}C_{1}$ chair, the GlcNAc pyranose ring explores the majority of conformational phase space and undergoes microsecond-timescale $^{4}C_{1} \leftrightarrow {}^{1}C_{4}$ puckering, the kinetics of which are modified by substituents. These predictions were consistent with our observations from NMR and the Protein Data Bank (PDB), which suggest that non-$^{4}C_{1}$ GlcNAc puckers are important in protein interactions. The simulations complete our computational studies of equilibrium puckering for the major hexosamine and uronic acid (Sattelle et al. 2010) constituents of HS. They also provide fundamental information to the wider glycobiology field by demonstrating the great potential of extended unperturbed aqueous simulations to facilitate rational modification of carbohydrate puckering kinetics and concomitant bioactivity. Our detailed analysis and 3D model of the equilibrium GlcNAc conformation in water can be used to drive the development of novel biotechnologies.

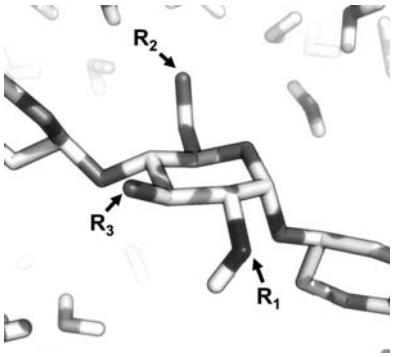

Fig. 1. Schematic of the GlcNAc scaffold in biological conditions. This ubiquitous carbohydrate building block, four derivatives from HS and their methylglycosides were studied using 20 μs simulations and 900 MHz NMR. For GlcNAc, R_1 = Ac, R_2 = H, R_3 = H; for GlcNS, $R_1 = SO_3^-$, R_2 = H, R_3 = H; for GlcNS6S, $R_1 = SO_3^-$, $R_2 = SO_3^-$, R_3 = H; for GlcNS6S3S, $R_1 = SO_3^-$, $R_3 = SO_3^-$, $R_3 = SO_3^-$; for GlcNS3S, $R_1 = SO_3^-$, R_2 = H, $R_3 = SO_3^-$.

Results

Pyranose ring puckering kinetics were investigated in *O*-sulfonated, *N*-sulfonated and *O*-methylated GlcNAc using microsecond all-atom explicit solvent MD simulations. Calculations were performed on the monosaccharides GlcNAc, GlcNS, GlcNS6S, GlcNS6S3S and GlcNS3S as free reducing sugars (the α-anomer) and α-1-*O*-methylglycosides (1-OMe). The simulations were initiated in both the $^{4}C_{1}$ and $^{1}C_{4}$ chairs and performed for 10 μs each. Thermodynamic equilibrium was confirmed by comparing averages of the Cremer–Pople θ-parameter (Sattelle et al. 2010); when convergence had occurred, both simulations (a total of 20 μs) were used in further analysis.

Microsecond-conformational exchange in GlcNAc

In the GlcNAc simulations, equilibrium of ring pucker was realized within 3–5 μs. As expected, the $^{4}C_{1}$ chair was the dominant conformer, present for 99.6% of the trajectory. The average Cremer–Pople puckering parameters for these $^{4}C_{1}$

conformers were: $Q = 0.54$ (±0.04) and $\theta = 10.1°$ (±5.5°). The hydroxyl groups were calculated to have the following preferences: O1 (*t*, 69%; *g*+, 19%; *g*–, 12%), O3 (*t*, 65%; *g*+, 22%; *g*–, 13%), O4 (*t*, 71%; *g*+, 18%; *g*–, 11%) and O6 (*t*, 67%; *g*+, 20%; *g*–, 13%). The hydroxymethyl populated the *gg* (59%), *gt* (39%) and *tg* (2%) conformers and the acetamido group was trans (165 ± 25°). For comparison, the experimental hydroxymethyl rotamer populations were estimated from the two experimental measurements ($J_{5,6proR}$ and $J_{5,6proS}$, Table I) and a three-site model to be: *gg* (96%), *gt* (4%) and *tg* (0%).

Ring and acetamido vicinal couplings of the free reducing GlcNAc α-anomer were accurately measured from 900 MHz [^{1}H]-1D NMR spectra in water. The $^3J_{2,3}$, $^3J_{3,4}$, $^3J_{4,5}$ and $^3J_{HN,H2}$ values were in the range 8–10 Hz, the $^3J_{1,2}$ coupling was ~3 Hz (Table I). Compared with experimental values, the computed ring vicinal couplings $^3J_{1,2}$ and $^3J_{2,3}$ were smaller, $^3J_{3,4}$ was identical and $^3J_{4,5}$ and $^3J_{HN,H2}$ were greater in magnitude. Computed values of $^3J_{5,6}$ were also very similar to NMR measurements, one being smaller and one larger. Since the calculated values were all within 1 Hz of experiment and the deviations were not systematic, errors could be assumed to propagate from either the Karplus equations used or the force-field parameters (less likely as these would be expected to be systematic across sets of couplings). Calculation of ring vicinal couplings from only GlcNAc $^4C_1$ conformers (99.6% of the trajectory) gave identical results. This comparison suggested that the simulation and the ensemble of predicted puckers were consistent with experiment.

Table I. Observed (Obs.) and calculated (Calc.) three-bond proton–proton vicinal couplings ($J_{H,H}$, Hz) for the five α-D-monosaccharides in water

Hexosamine	Coupling	Obs.	Calc.
GlcNAc	$J_{1,2}$	3.5	3.2
GlcNAc	$J_{2,3}$	10.7	10.1
GlcNAc	$J_{3,4}$	9.9	9.9
GlcNAc	$J_{4,5}$	9.3	10.0
GlcNAc	$J_{HN,H2}$	8.8	9.7
GlcNAc	$J_{5,6proR}$	5.2[a]	4.5
GlcNAc	$J_{5,6proS}$	2.3[a]	3.2
GlcNS	$J_{1,2}$	3.5	2.6
GlcNS	$J_{2,3}$	10.4	10.2
GlcNS	$J_{3,4}$	9.0	9.9
GlcNS	$J_{4,5}$	10.2	10.0
GlcNS6S	$J_{1,2}$	3.5	2.6
GlcNS6S	$J_{2,3}$	10.4	8.8
GlcNS6S	$J_{3,4}$	9.1	9.8
GlcNS6S	$J_{4,5}$	10.1	9.9
GlcNS6S3S	$J_{1,2}$	3.3	2.7
GlcNS6S3S	$J_{2,3}$	10.7	10.2
GlcNS6S3S	$J_{3,4}$	8.9	8.3
GlcNS6S3S	$J_{4,5}$	10.1	10.0
GlcNS3S	$J_{1,2}$	3.3	2.7
GlcNS3S	$J_{2,3}$	10.7	10.2
GlcNS3S	$J_{3,4}$	8.8	9.9
GlcNS3S	$J_{4,5}$	10.1	8.5

The Karplus equations of Hricovini and Bizik, Altona and Haasnoot (1980) and Mobli and Almond (2007) were used for pyranose ring, hydroxymethyl and acetamido vicinal couplings, respectively. Experimental errors were estimated to be ±0.2 Hz and standard deviations of calculated ring vicinal couplings were estimated to be at most 0.01 Hz. (except GlcNAc $J_{5,6proR}$ which was ±0.1 Hz).
[a]Data from a previous NMR study (Blundell et al. 2009).

All of the $^4C_1$ hemisphere and boat and skew boat (equatorial) canonical puckers were populated in the simulation of GlcNAc. Although the $^4C_1$ pucker was dominant, the $^1C_4$ chair was also transiently occupied, with averages $Q = 0.52$ (±0.04) and $\theta = 166.3°$ (±6.5°). The computed pathway between the two chairs involved predominantly $^4C_1 \leftrightarrow {}^2H_3 \leftrightarrow {}^2S_O \leftrightarrow {}^1S_3 \leftrightarrow {}^1S_5 \leftrightarrow {}^5H_4 \leftrightarrow {}^1C_4$; however, 27 of the 36 canonical non-chair puckers were populated (Figure 2). A total of 16 $^4C_1 \rightarrow {}^1C_4$ transitions were observed (Figure 3), occurring at a computed (forward) rate of 0.8 μs^{-1}. The average lifetime of the GlcNAc $^1C_4$-chair puckers was ~3 ns, giving a $^1C_4 \rightarrow {}^4C_1$ (backward) rate of 292 μs^{-1} and an equilibrium constant of $K_{eq} = 2.9 \times 10^{-3}$ (assuming first-order kinetics). Using the simulated equilibrium data, the GlcNAc $^4C_1$ chair was lower in free energy than the $^1C_4$ chair, by $\Delta G = 3.5$ kcal mol^{-1}. The dominant non-chair puckers in the $^4C_1$ hemisphere were half-chairs and envelopes with either C2 up or C3 down ($^2H_3$, ^2E, $^2H_1$ and E_3). Three transition states between skew boats and the $^1C_4$ chair were predicted; namely, the unstable envelopes and half-chair conformers E_4, $^5H_4$ and ^5E. Representative 3D structures of the key $^4C_1$- and $^1C_4$-hemisphere intermediates from the simulation are illustrated in Figure 4. Transition to the ^2S_O-conformer allowed facile pseudorotation in the equatorial region. The primary boat and skew boat puckers were those with φ-values in the range 150–330°; the most populated were ^2S_O, $B_{3,O}$, $^1S_3$ and $^OS_2$ (Figure 5). However, conversion to the $^1C_4$ chair occurred from the much less populated $^{1,4}B$, $^1S_5$ and $B_{2,5}$ conformers (Figure 6).

*The effect of 1-*O*-methylation: a model for polymerization*

Simulations of 1-OMe-GlcNAc reached a conformational equilibrium after ~3–5 μs. Consistent with the free reducing α-anomer simulation, a range of puckers were predicted (28 of the 36 non-chair canonical conformers, Figure 2) with the $^4C_1$ chair as the major conformer. The average $^4C_1$ pucker for 1-OMe-GlcNAc had values of $Q = 0.56$ (±0.04) and $\theta = 9.7°$ (±5.3), similar to GlcNAc. Five $^4C_1 \rightarrow {}^1C_4$ transitions were predicted and their computed pathway was similar to that of the free α-anomer; however, differences in the population of conformers were predicted (Figure 6B). Neighboring the $^4C_1$ pucker, envelopes and half-chairs with either O5 up or C1 down (^OE, $^OH_1$, E_1 and $^2H_1$) were more populated in the 1-OMe-GlcNAc simulation. Those with C2 up or C3 on down (^2E, $^2H_3$, E_3 and $^4H_3$) and with C4 up or C5 down (^4E, $^4H_5$, E_5 and $^OH_5$) were less populated than in GlcNAc. This trend in equatorial conformer populations was identical to GlcNAc; however, all puckers except $^1S_3$ were less populated. In particular, the population of $B_{2,5}$ was almost precluded by the 1-*O*-methylsubstitution (Figures 2 and 6B). In the $^1C_4$ hemisphere, compared with the GlcNAc simulation, the envelope E_4 was less populated, $^5H_4$ was more populated and ^5E was absent in the methylglycoside simulation. Calculated orientations of the hydroxyl, hydroxymethyl and acetamido groups were identical to those computed for GlcNAc. In contrast, the rate of $^4C_1 \leftrightarrow {}^1C_4$ transition was reduced in the 1-OMe-GlcNAc simulation (cf. GlcNAc). Forward and backward rates were computed to be 0.3 and

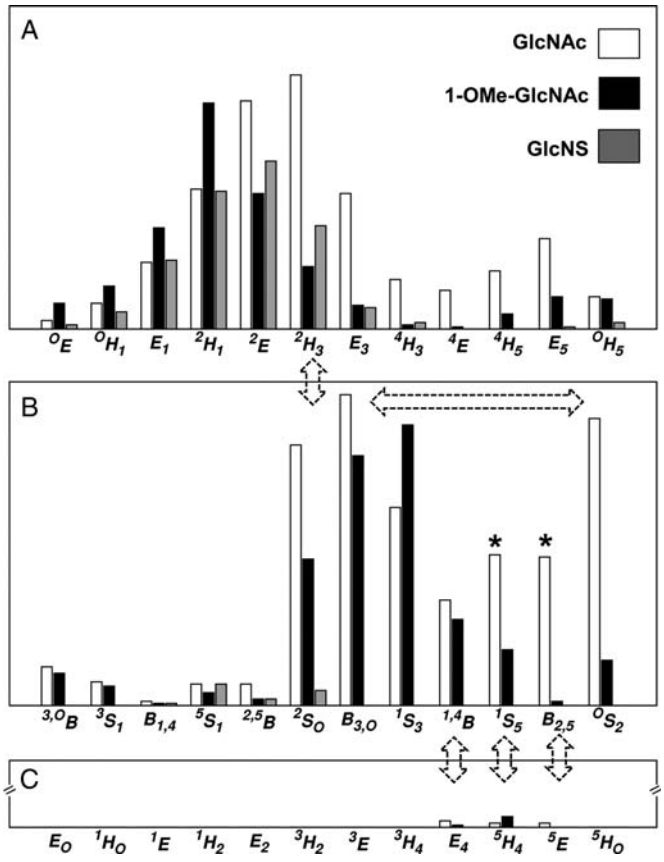

Fig. 2. Relative occupancy (*y*-axis, arbitrary units) of the 36 canonical non-chair conformers in the 20 μs explicit solvent simulations of GlcNAc, 1-OMe-GlcNAc and GlcNS. (**A**) $^{4}C_1$ hemisphere, (**B**) equatorial region and (**C**) $^{1}C_4$ hemisphere. Dashed arrows highlight predicted transitions between polar and equatorial regions and pseudorotation. Asterisks denote intermediates notably suppressed by 1-*O*-methyl and *N*-sulfo substituents.

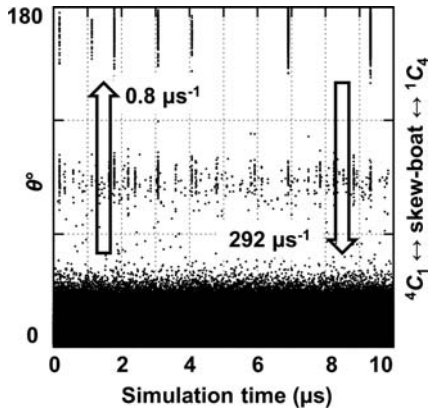

Fig. 3. Evidence for microsecond-timescale puckering in aqueous GlcNAc. The $^{4}C_1 \leftrightarrow {}^{1}C_4$ transitions, computed exchange rates and short-lived (~3 ns) $^{1}C_4$-chair puckers are shown on a time-series plot of the Cremer–Pople parameter θ. Data are from the 10 μs $^{4}C_1$-initiated explicit solvent GlcNAc simulation.

146 μs^{-1}, respectively, which resulted in a calculated equilibrium constant of $K_{eq} = 1.9 \times 10^{-3}$. Using this equilibrium data, the $^{4}C_1$ chair was calculated to be $\Delta G = 3.7$ kcal mol^{-1} lower in free energy than the $^{1}C_4$ chair. Therefore, the two chair conformers in GlcNAc and 1-OMe-GlcNAc had similar equilibria and relative free energies, but methylation slowed the conformational exchange kinetics.

Quantum mechanical (QM) energy calculations were performed to further explore the relative energies of the chair puckers and the energy barriers separating them, in the absence of explicit solvent. The GlcNAc $^{4}C_1$ pucker was predicted by QM to be 19.1 kcal mol^{-1} lower in energy than the $^{1}C_4$ conformer and the lowest energy equatorial pucker, $^{1}S_3$ ($\varphi = 213°$), was 11.4 kcal mol^{-1} above the $^{4}C_1$ chair. For 1-OMe-GlcNAc, the two chairs were separated by 16.8 kcal mol^{-1} and the lowest energy equatorial pucker, $^{1}S_5$ ($\varphi = 270°$), was 11.4 kcal mol^{-1} above the $^{4}C_1$ pucker energy. The QM calculations trended in agreement with the MD simulations with respect to the most likely predicted pathway of $^{4}C_1 \leftrightarrow {}^{1}C_4$ exchange. The magnitude of predicted relative energies was lower in MD than QM calculations and inclusion of implicit solvent exacerbated the disagreement (the energy difference between chairs increased to 21.6 and 20.3 kcal mol^{-1} for GlcNAc and 1-OMe-GlcNAc, respectively). Furthermore, QM predicted the $^{2}S_O$ pucker (abundantly populated in aqueous simulations) to be the highest energy equatorial pucker (30 kcal mol^{-1} above the $^{4}C_1$ chair energy) in both GlcNAc and 1-OMe-GlcNAc.

The effects of sulfonation on microsecond dynamics

In the case of GlcNS (*N*-sulfonated free α-anomer), the simulations equilibrated to an essentially 100% $^{4}C_1$ conformation (Figure 7A), which had an average pucker of $Q = 0.55$ (±0.04) and $\theta = 9.5°$ (±5.2). When initiated in the $^{1}C_4$ pucker, the molecule rapidly exchanged to the $^{4}C_1$ chair (during the 250

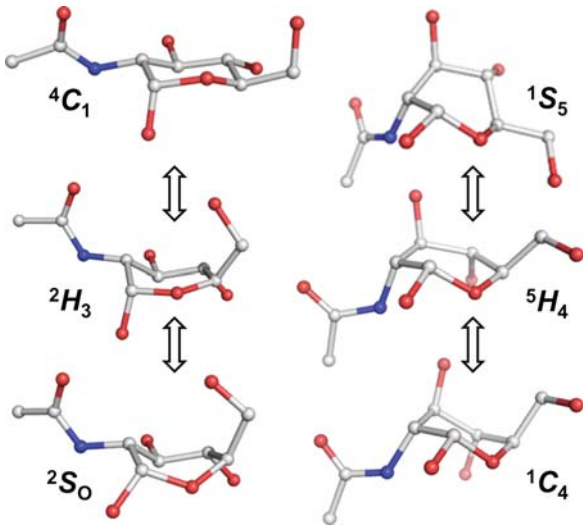

Fig. 4. Representative GlcNAc conformers from the 20 μs explicit solvent simulation involved in transitions between chairs and skew boats. Hydrogen atoms are hidden for clarity.

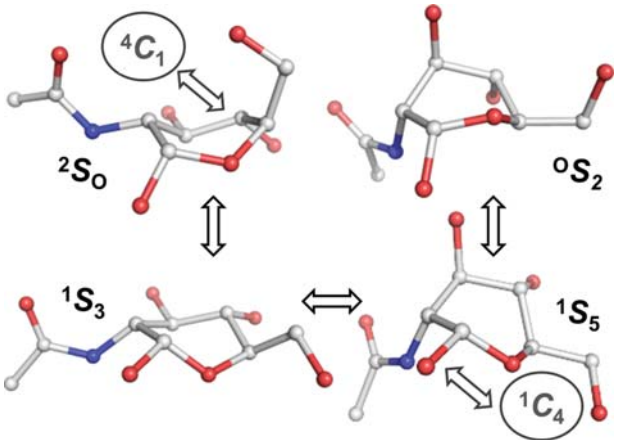

Fig. 5. Representative GlcNAc skew boat conformers involved in pseudorotation; the structures were derived from a 20 μs explicit solvent simulation. Hydrogen atoms are hidden for clarity.

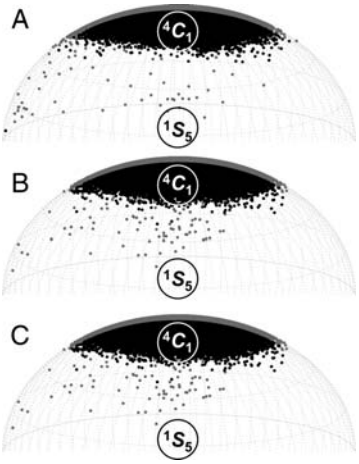

Fig. 7. Conformational space of free α-anomer hexosamines that explored only the $^4C_1$ hemisphere of Cremer–Pople phase space during the 20 μs explicit solvent simulations: (**A**) GlcNS, (**B**) GlcNS3S and (**C**) GlcNS6S3S. Each hemisphere is orientated, labeled and colored as in Figure 6.

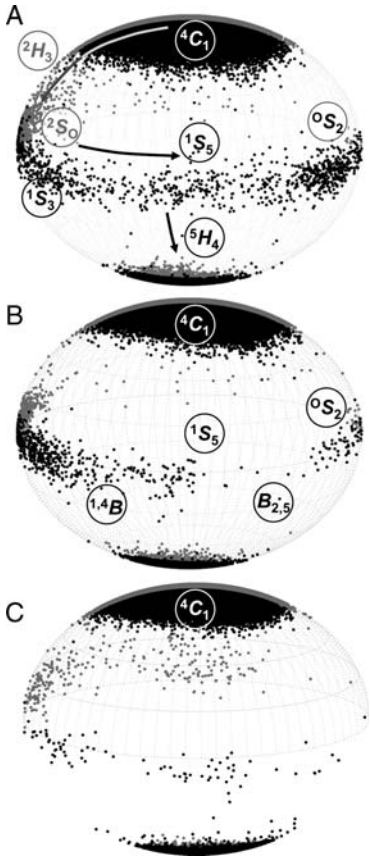

Fig. 6. Conformers explored by hexosamines that underwent $^4C_1 \leftrightarrow {}^1C_4$ transitions during 20 μs explicit solvent simulations: (**A**) GlcNAc, (**B**) 1-OMe-GlcNAc and (**C**) GlcNS6S. Puckers are plotted in spherical Cremer–Pople phase space with the $^1S_5$-conformer orientated at the front. Hence, data points at the front (black) and back (gray) of the sphere denote puckers with φ-values in the range 180–360° and 0–180°, respectively. The skew boat and boat labels (*S* and *B*, respectively) are situated above or below their positions on the equator. The half-chairs (*H*) are labeled adjacent to their positions on the sphere.

ns discarded equilibration phase) and did not return to the $^1C_4$ conformation. The *N*-sulfo substitution did not significantly perturb the distribution of rotamer states at the hydroxyl and hydroxymethyl groups (cf. GlcNAc) and the *N*-sulfonyl occupied three distinct acetamido rotamer states, centered on +60, −90 and −160°. Computed and experimental pyranose ring vicinal couplings were in excellent agreement. As for GlcNAc, all calculated values were within 1 Hz of the experimentally measured value (Table I). In contrast to the GlcNAc simulation, only a small number of canonical puckers were observed other than $^4C_1$ (Figure 2); the most populated of these were the envelopes and half-chairs with C2 up (^2E, $^2H_1$ and $^2H_3$). The only GlcNS boats and skew boats had φ-values in the rather limited range 90–150°, which were $^5S_1$, ^2S_O, $^{2,5}B$ and $B_{1,4}$. No transition states were predicted between these puckers and the (unpopulated) $^1C_4$ chair. For 1–OMe-GlcNS, the $^1C_4$-initiated trajectory remained in the $^1C_4$ chair for several hundred nanoseconds. During the remaining simulation time, no transitions were observed from $^4C_1$ to $^1C_4$. Thus, it was concluded that the kinetic rate for exchange between the two chair forms had been slowed significantly due to *N*-sulfonation and further still by methylation.

Using QM, the relative energy of the two GlcNS chairs was 3.0 kcal mol^{-1} (cf. 13.8 kcal mol^{-1} using implicit solvent), with the $^4C_1$ chair lower in energy. Notably, the GlcNS $^4C_1$ chair and the equatorial $B_{2,5}$ pucker ($\varphi = 300°$) were predicted by QM to be energetically degenerate, which was at odds with the explicit solvent MD simulations. The $^{1,4}B$ conformer ($\varphi = 240°$) was just 1.6 kcal mol^{-1} above the $^4C_1$ chair and three $^4C_1$-hemisphere puckers (with θ in the range 150–170° and φ in the range 240–270°) were computed by QM to be within 3.0 kcal mol^{-1} of the $^4C_1$ chair.

In the case of the GlcNS6S free α-anomer, this molecule was predicted to be a stable $^4C_1$ chair with average *Q*- and θ-values of 0.55 (±0.04) and 9.5° (±5.2), respectively. In the $^4C_1$-initiated simulation of GlcNS6S, a single $^4C_1 \leftrightarrow {}^1C_4$ transition occurred after ~6 μs (Figure 6C), in which the $^1C_4$ chair was populated for ~160 ns. Thus, the backward

exchange rate was estimated to be ~6 μs^{-1}. Assuming the equilibrium constant remained at 3×10^{-3}, the rate of $^4C_1 \leftrightarrow {}^1C_4$ conformational exchange was estimated to be ~50 times slower in GlcNS6S than in GlcNAc, suggesting a forward rate of 0.02 μs^{-1} and explaining why so few transitions had been observed within even 20 μs. This finding also suggested that the activation free energy barrier was increased in GlcNS6S (cf. GlcNAc) by ~2.3 kcal mol^{-1}. Although the non-equilibrium GlcNS6S simulations precluded calculation of the relative energy between chairs, prediction of an accessible $^4C_1 \leftrightarrow {}^1C_4$ pathway in the $^4C_1$-initiated trajectory allowed further investigation by QM. The prediction that the two conformers and the equatorial $B_{2,5}$ pucker ($\varphi = 300°$) had the same energy was at odds with the MD simulations, in which $B_{2,5}$ was rather minimally populated compared with the $^5S_1$ and ^2S_O conformers ($\varphi = 90$ and 150°, respectively), both of which were predicted to be very unfavorable by QM (>30 kcal mol^{-1} above the $^4C_1$-chair energy).

For 3-*O*-sulfonated GlcNS3S and GlcNS6S3S, only the $^4C_1$ conformer was observed (Figure 7B and C). Again, exchange from the $^1C_4$ pucker occurred rapidly during the equilibration phase. Average *Q*-values for the $^4C_1$ conformers of these hexosamines were identical, 0.56 (±0.04), and the θ-values were 9.5 (±5.2) and 9.6 (±5.3) for GlcNS3S and GlcNS6S3S, respectively. All of the di- and tri-sulfonated hexosamines had computed vicinal couplings within 1 Hz of the measured value (Table I) with two exceptions, $^3J_{2,3}$ of GlcNS6S and $^3J_{4,5}$ of GlcNS3S, which were smaller than the corresponding experimental data by 1.2–1.6 Hz, suggesting that the abundance of sulfate groups had made the general Karplus equations used less accurate. Again, the hydroxyl rotamer states and hydroxymethyl conformations were identical in GlcNS3S and GlcNS6S3S compared with unsulfonated GlcNAc. In the 3–*O*-sulfonated GlcNS3S and GlcNS6S3S simulations, the *N*-sulfonyl group was different from GlcNS, being predicted to populate only two rotamer states (+60 and −160°), rather than the three found in GlcNS.

None of the $^4C_1$- or $^1C_4$-initiated sulfonated methylglycoside simulations reached conformational equilibrium. This was attributed to the extended time taken for the $^1C_4$-initiated trajectories to undergo the $^1C_4 \rightarrow {}^4C_1$ exchange. The $^1C_4$-pucker lifetime was correlated with the degree of sulfonation and estimated to be: 1-OMe-GlcNAc (<250 ns), 1-OMe-GlcNS (600 ns), 1–OMe-GlcNS3S (1.2 μs), 1-OMe-GlcNS6S (2.8 μs) and 1-OMe-GlcNS6S3S (5.7 μs). A lifetime of 5 μs corresponds to a back transition rate of 0.2 μs^{-1} or ~1000 times slower than in GlcNAc. Assuming the equilibrium constant was similar to GlcNAc, this equates to an increase in activation energy of ~4.1 kcal mol^{-1}. For the $^4C_1$-initiated simulations, which did not populate any $^1C_4$-hemisphere puckers, increased sulfonation resulted in an increased population of $^4C_1$-hemisphere envelopes and half-chairs. The $^2H_1$ half-chair was the most populated intermediate in all $^4C_1$-initiated simulations and envelopes E_1 and ^2E were the next most populated. Only boats and skew boats with φ-values in the range 60–150° ($B_{1,4}$, $^5S_1$, $^{2,5}B$ and ^2S_O) were occupied. Here, the $^5S_1$ conformer of 1-OMe-GlcNS6S3S was significantly more stable than in any of the other sulfonated methylglycosides. In the $^1C_4$-initiated trajectories, the distribution of transition states between skew boats and the $^1C_4$ chair was similar for the mono- and di-sulfonated hexosamines. However, for 1-OMe-GlcNS6S3S, the puckers $^5H_4$ and ^5E were much more populated. At the equator, puckers with φ-values in the range 270–330° ($^1S_5$, $B_{2,5}$ and $^OS_2$) were occupied by all of the sulfonated methylglycosides, although the $^1S_3$ and $^{1,4}B$ conformers were comparatively inaccessible to 1-OMe-GlcNS6S3S. The 1-OMe-GlcNS and 1–OMe-GlcNS6S3S $^1C_4$-initiated simulations were predicted to populate $B_{2,5}$ and $^OS_2$ almost equally and much more so than in 1-OMe-GlcNS6S and 1-OMe-GlcNS3S.

In the di- and tri-sulfonated free reducing and methylglycoside hexosamines ($^1C_4$-initiated trajectory), the sulfo moieties rearranged during the single transition to the favored $^4C_1$ pucker. This transition brings all of the sulfo groups from the axial to the equatorial position with a consequent increase in the distance from the 6-*O*-sulfo to both *N*- and 3-*O*-sulfo. For example, in 1–OMe-GlcNS6S3S, these distances increased on average by ~1 Å (Figure 8) and the distance between the adjacent *N*- and 3-*O*-sulfo moieties decreased slightly following the transition. These observations indicate that solvation forces and electrostatic repulsion between sulfo groups play an important role in favoring the $^4C_1$ pucker over $^1C_4$.

Analysis of crystallographic data

In an analysis of crystallographic high-resolution (≤2.0 Å) PDB GlcNAc depositions, 96.9% of the 3137 occurrences were in the $^4C_1$ conformation. However, 0.5% were $^1C_4$ puckers and 2.6% were boats or skew boats, such as in the non-enzyme structures of viral hemagglutinin, SNA-II, CD2 and interlukin-19 (Ikemizu et al. 1999; Chang et al. 2003; Maveyraud et al. 2009; Xu et al. 2010). For the $^4C_1$ conformers, average puckering parameters were $Q = 0.57$ and $\theta = 9.1°$; in the $^1C_4$ conformers, the averages were $Q = 0.59$ and $\theta = 163°$. For reference, average values from our simulations were as follows: $^4C_1$ puckers: $Q = 0.54$ (±0.04), $\theta = 10.1°$ (±5.5°); and $^1C_4$ puckers: $Q = 0.52$ (±0.04), $\theta = 166°$ (±6.5°). From the Cambridge Structural Database (CSD), the two entries for free α-D-GlcNAc [ACGLUA10 (Johnson 1966) and ACGLUA11 (Mo and Jensen 1975)] are $^4C_1$ chairs; they exhibit *Q*-values of 0.62 and 0.58, with respective θ-values of 7.6 and 3.1°. In the recent 1 Å resolution crystal structure of chitin (Nishiyama et al. 2011), the GlcNAc θ parameter is identical to the simulation $^4C_1$ average (10°). Sulfonated hexosamines were also found in these repositories. For GlcNS6S, 16 ligands were identified in 13 crystallographic PDB depositions (≤2.0 Å resolution), 12 were $^4C_1$ chairs, 3 were $^1C_4$ chairs and 3 were equatorial conformers. Average puckering parameters in the $^4C_1$ conformers were $Q = 0.59$ and $\theta = 10.3°$; our computed data for this GlcNS6S pucker were $Q = 0.55$ (±0.04) and $\theta = 9.5°$ (±5.2°). In the CSD, two GlcNS molecules were identified [ZULPIF (Ojala et al. 1995) and ZULPIF01 (Yates et al. 1995)], which exist as $^4C_1$ chairs and have *Q*-values of 0.56 and 0.55 and θ-values 4.0 and 2.9°, respectively.

Discussion

Extended-timescale simulations can exaggerate even small force-field inaccuracies and lead to errors in 3D-structural

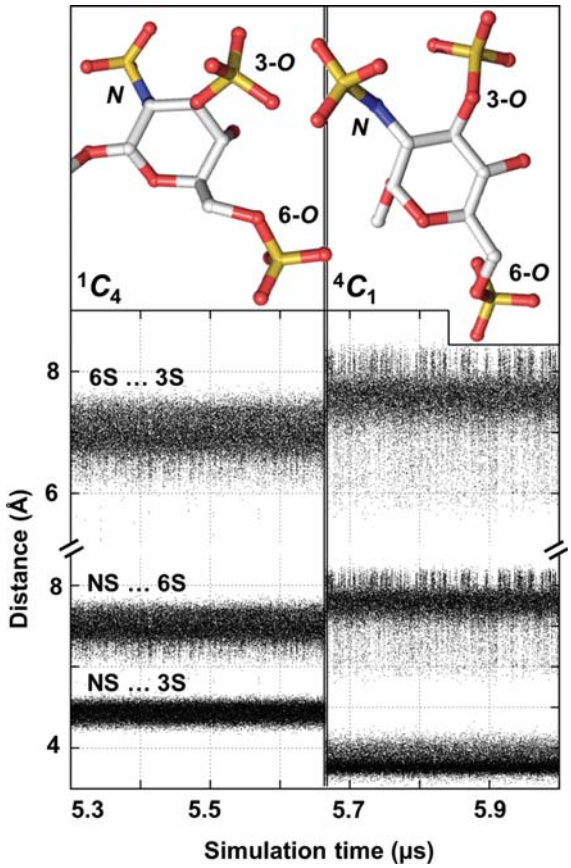

Fig. 8. Evidence that electrostatic repulsion contributes to stabilization of the $^4C_1$ chair in highly sulfonated hexosamines. In the case of the 10 μs $^1C_4$-initiated methylglycoside GlcNS6S3S explicit solvent simulation, time-series plots illustrate the change in distances between sulfur atoms resulting from the single $^1C_4 \rightarrow {}^4C_1$ transition after ~5.6 μs. Representative 3D structures of $^1C_4$ and $^4C_1$ chairs show how conformational rearrangement increased the distance between NS/6S and 3S/6S sulfate pairs. Hydrogen atoms were hidden for clarity.

ensembles (Orozco et al. 2008; Klepeis et al. 2009). Comparison with experiment suggested that our simulations, using GLYCAM06, did not suffer from this phenomenon (Table I) and, in the cases of GlcNAc and 1-OMe-GlcNAc, equilibration of puckering in took ~3–5 μs. Although in polymers the timescale of equilibration may differ, this finding suggests that previous (nanosecond) GlcNAc simulations explored only a small fraction of conformational phase space. Consequently, previous thermodynamic and kinetic interpretations of simulated GlcNAc puckering should be treated with caution. Importantly, the predicted microsecond-timescale exchange between GlcNAc chair puckers was not in disagreement with NMR measurements reported here (Table I) and elsewhere (Mulloy and Johnson 1987; Jin et al. 2009).

Average Q- and θ-values for chair puckers of GlcNAc and GlcNS6S from the simulations were similar to their respective values derived from the PDB, whereas GlcNAc was identical to a 1 Å resolution 3D structure of chitin (Nishiyama et al. 2011). The CSD data for GlcNAc and GlcNS, derived from crystals devoid of water and protein, were slightly more rigid than our predictions. The trend for non-$^4C_1$ puckers of GlcNAc in the PDB and our simulations was similar. Our comparisons of calculated and experimental data provide confidence that the simulated puckering was representative of real conformational exchange in GlcNAc and its derivatives. Furthermore, these similarities support the view that, while GlcNAc exists predominantly as a $^4C_1$ chair in water, other puckers may be biologically important, particularly in unsulfonated GlcNAc.

Our QM data of GlcNAc conformers (without explicit solvent) were consistent with previous studies, such as those of glucose (Barrows et al. 1995; Appell et al. 2004), but in general provided larger relative chair energies than MD and also predicted a different set of boat and skew boat intermediates. However, it should be noted that energies computed without water may be sensitive to small geometrical perturbations due to unnatural intramolecular hydrogen bonding and the large relative QM energies may be a consequence of this. For example, QM predicted GlcNAc to be a rigid $^4C_1$ chair, whereas MD suggested the barrier height was ~5 times the thermal energy at room temperature, which is in close agreement with many other studies of pyranoses (Dowd et al. 1994; Barnett and Naidoo 2010; Barnett et al. 2010; Spiwok et al. 2010). The finding that the majority of conformational phase space was computed to be accessible in GlcNAc, including the $^1C_4$ chair, also challenges the notion that GlcNAc is rigid. We now propose that aqueous GlcNAc undergoes microsecond-timescale conformational exchange, which would not be concluded from straightforward interpretation of NMR vicinal couplings, sub-microsecond unequilibrated MD and gas-phase QM energy calculations. Whether similar conclusions would be made for other biologically important hexosamines, such as *N*-acetyl-D-galactosamine, remains to be seen.

The hypothesis that GlcNAc undergoes room-temperature-accessible microsecond timescale $^4C_1 \leftrightarrow {}^1C_4$ transitions (separated by $\Delta G = 3.5$ kcal mol^{-1}) that are consistent with protein co-crystals, but which cannot be predicted by gas phase or implicit solvent QM calculations (in which the chair forms were predicted to be 19.1 kcal mol^{-1} different), suggests a major role for water in stabilizing the ensemble of GlcNAc puckers. It has been theorized that water is essential to predict carbohydrate conformation (Kirschner and Woods 2001) and our data concurs. As concluded previously (Sattelle and Almond 2010), we again found that extensive empirical simulations were preferential to restricted studies at higher levels of theory for carbohydrates, due to their ability to resolve microsecond dynamics. Figure 9 illustrates the 3D structure of GlcNAc with the pucker and substituents in the most frequently encountered conformation in the 20 μs simulation. This 3D model (available as Supplementary data) could be used as $^4C_1$-dictionary data for structural refinement, protein docking or structure-based design.

In the absence of unambiguous atomic-resolution experimental data and extended aqueous simulations, it has not been possible to robustly quantify equilibrium conformer populations or the kinetics of puckering exchange at the molecular level. Our simulations of GlcNAc and uronic acid

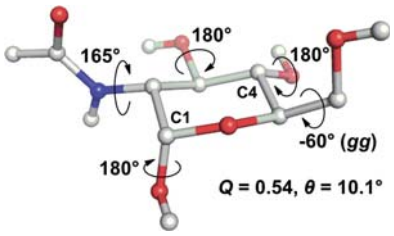

Fig. 9. A 3D model for the equilibrium GlcNAc conformation in water. The pucker is a $^4C_1$ chair, the pyranose conformation and rotamer states (hydroxyl, hydroxymethyl and acetamido) represent the most populated in a 20 μs explicit solvent simulation. Non-polar hydrogen atoms are hidden for clarity and the 3D coordinates are provided in Supplementary data S4.

derivatives (Sattelle et al. 2010) clearly demonstrate that recent progress in computer hardware and software (Harvey et al. 2009; Klepeis et al. 2009) has enabled conformationally equilibrated simulations to be performed for carbohydrates involved in microsecond-puckering exchange without the need for enhanced sampling (i.e. artificial perturbation of the simulation temperature or Hamiltonian; Gao et al. 2008). Although enhanced sampling is useful for predicting equilibrium populations, biological interpretation of kinetic phenomena should be treated with caution (Schlick 2009).

Neither the methylglycoside nor the *N*- or *O*-sulfo derivative was predicted to alter the rotational preferences of hydroxyl or hydroxmethyl groups. The simulations suggested that the effect of these substituents was instead to add steric bulk and charge, and hence to modify pyranose ring puckering. The methylglycoside has previously been shown to influence pyranose conformation (Marszalek et al. 1998; Heymann and Grubmuller 1999; Li et al. 1999), and this reinforces our thesis that knowledge of equilibrium populations and kinetics are crucial for a complete understanding of carbohydrate 3D SARs. For example, the slower rate of $^4C_1 \rightarrow {}^1C_4$ transition in 1-OMe-GlcNAc (three times cf. GlcNAc) implied a 0.4 kcal mol^{-1} increase in activation energy. This was found to be due to the relative inaccessibility of several intermediates in 1-OMe-GlcNAc, and in particular ^2S_O, $^1S_5$ and $B_{2,5}$ (Figures 2 and 6), indicating a higher-energy barrier to pseudorotation. Sulfonation further increased this energy barrier, making it more difficult for the $^1C_4$-initiated methylglycosides to the exchange from this pucker to the $^4C_1$ chair.

The equilibrium of GlcNS puckers was shifted toward the $^4C_1$ chair (cf. GlcNAc). Puckers involved in the transition between GlcNAc $^4C_1$ and $^1C_4$ chair conformers were largely precluded in GlcNS (except for ^2S_O), implying that *N*-sulfonation significantly slows the rate of $^4C_1 \leftrightarrow {}^1C_4$ conformational exchange by blocking these intermediates. The *N*-sulfo substituent is ubiquitous in HS, where GlcNAc is sequentially modified by *N*-deacetylase and *N*-sulfotransferase enzymes prior to sequential *O*-sulfotransferase-catalyzed sulfonation at the 6-*O*- and 3-*O*-positions (Rabenstein 2002). Our results intimate that this modification both rigidifies and stabilizes the $^4C_1$ pucker of HS GlcNAc residues.

Rearrangement of sulfo groups from the axial to the more solvent-favorable equatorial orientation is probably a major driver of the $^1C_4 \rightarrow {}^4C_1$ transition in the di- and tri-sulfonated hexosamines orientations. However, the distance between sulfo groups also increased as a result of this transition, suggesting that it was partially driven by electrostatic repulsion (Figure 8). Together, these observations infer that puckering of the GlcNAc pyranose scaffold is strongly dependent on sulfo substituents and polymerization, but further studies are required to confirm this. Such insights will facilitate molecular design by making it possible to predict substitutions that perturb the aqueous conformational equilibrium, rates of puckering and concomitant bioactivity. For example, based on our simulations, we now hypothesize that GlcNAc glycosides more bulky than a methyl group would further decrease the rate of $^4C_1 \leftrightarrow {}^1C_4$ conformational exchange in water.

Equilibration of pucker was realized on the same timescale as seen previously for uronic acids (Sattelle et al. 2010), but the predicted 1-OMe-GlcNAc forward ($^4C_1 \rightarrow {}^1C_4$) exchange rate (0.3 μs^{-1}) was much slower than in 1-OMe-IdoA (19 μs^{-1}), again indicating that epimerization at the C5 position significantly lowers the barrier to kinetic exchange of pucker. In both GlcNAc and IdoA, the $^1C_4$ conformer was computed to be accessible at room temperature; the key difference was the kinetics of exchange, which was slower in GlcNAc due to the relatively-higher free energy of the $^1C_4$ pucker (~3 kcal mol^{-1} higher than in IdoA). The effect of IdoA2S on 1-OMe-IdoA was to shift the equilibrium conformation toward the $^1C_4$ pucker (1-OMe-IdoA and 1-OMe-IdoA2S were predicted to be 76 and 91% $^1C_4$, respectively), whereas in C5-epimerised and *N*-acetylated GlcNAc, *N*-, 6-*O*- and 3-*O*-sulfonation favored the $^4C_1$ chair. Furthermore, the studies performed here suggest that our previous work on methylglycosides of uronic acids may be more representative of puckering exchange rates in polysaccharides than monosaccharides. Together, these data provide a basis for understanding glycosaminoglycan 3D structure.

Characterization of glycosaminoglycan 3D structures will enable the design of biotechnological devices and medicines (Gama et al. 2006; Ghosh et al. 2009). The predicted substituent dependence of GlcNAc puckering, and that of uronic acids (Sattelle et al. 2010), leads us to hypothesize that the slower exchange kinetics of sulfonated GlcNAc residues (favoring a more rigid $^4C_1$ chair) may, in concert with electrostatic repulsion of sulfo moieties, contribute to the observation that HS S-domains are more rigid than NA-domains (Mobli et al. 2008). The simulations also suggest that puckering could have a significant effect on HS-domain structure by altering chain direction, and it is conceivable that it has a more dominating effect on bioactivity than the glycosidic linkage motions, which are unperturbed by sulfonation (Mulloy and Forster 2000). Insight into the relative contribution of microscopic uronic acid and hexosamine puckering to macroscopic HS-domain 3D structure will be gained from future conformationally equilibrated (microsecond-timescale) co-polymer simulations. It will be interesting to establish if bioactivity of the therapeutically relevant HS motif $(GlcNS6S\text{-}IdoA2S)_3$ (Smits et al. 2010) and the heparin pentasaccharide are modulated by incorporation of conformationally locked GlcNAc derivatives, as is the case for heparin derivatives exhibiting ^2S_O-biased IdoA2S (Das et al. 2001; Boltje et al. 2009). It has been proposed that IdoA flexibility

does not affect the molecular shape of heparin (Jin et al. 2009). Although not inconsistent with our data, this conclusion was derived from 4 ns of restrained MD or 0.1% of the ~3 μs now known to be required to equilibrate puckering (explore all conformational phase space) in monosaccharides studied to date, and the analogous effect of GlcNAc puckering has not yet been considered.

Substituent-dependent microsecond-timescale puckering in GlcNAc has important ramifications in wider glycobiology. Despite being rare events, the proposed $^4C_1 \leftrightarrow {}^1C_4$ transitions equate to ~1 million s^{-1} in GlcNAc and we therefore hypothesize that they may be an important factor in protein selectivity. In total, 75% of canonical non-$^4C_1$ puckers were predicted to be accessible for this hexosamine in water at room temperature. High-resolution data from the PDB suggest that non-$^4C_1$ puckers may play an important role in protein recognition and carbohydrate catalysis. For example, ATIII prefers the ^2S_O-skew boat of IdoA2S in heparin (Hricovini et al. 2001), β-mannosidases bind their substrate in the $^1S_5$ conformation (Ardevol et al. 2010) and cellobiohydrolase I of *Trichoderma reesei* drives the envelope and half-chair conformations (^4E and $^4H_3$) of glucose and renders both chair conformers highly unfavorable (Barnett et al. 2010).

Knowledge of puckering in GlcNAc will lead to new molecular design opportunities. For example, GlcNAc is an essential constituent of protein post-translational modifications (Marino et al. 2010; Nothaft and Szymanski 2010). Rational modification of epitope GlcNAc puckering kinetics can be expected to modulate protein recognition and thereby facilitate development of therapeutics (Jefferis 2009). Also, there are no available 3D structures of *Rhizobium* nodulation factors, which are characterized by a backbone of between three and five substituted (sulfonated) GlcNAc residues. Recent work has begun to address this knowledge gap with NMR and nanosecond-simulations (Morando et al. 2011). Definition of nodulation factor SARs and generation of synthetic derivatives will accelerate production of non-leguminous plants that can fix nitrogen themselves, toward which our extended microsecond-simulations now contribute. Our predictions also provide a new avenue for development of novel peptidoglycans (for amelioration of bacterial pathogenicity) and biomaterials from marine carbohydrates and chitin (Khoushab and Yamabhai 2010). Furthermore, understanding equilibrium conformer populations and the kinetics of exchange in atomic detail, as has been described, will rationalize decision-making in structure-based design and facilitate generation of increasingly high-affinity, typically weak-binding, carbohydrate-based ligands.

Conclusions

The longest carbohydrate simulations to date were performed on the ubiquitous monosaccharide GlcNAc and biologically important derivatives to investigate microsecond dynamics that cannot currently be quantified by experiments or other computational approaches. In water, at equilibrium, GlcNAc underwent microsecond-timescale exchange between chair puckers, in good agreement with NMR measurements and high-resolution crystallographic data for protein-bound GlcNAc ligands, where an appreciable number are not $^4C_1$ conformers. These results challenge the hypothesis that GlcNAc is a perfectly rigid $^4C_1$ chair, as predicted by high-level energy calculations without explicit water, straightforward interpretation of NMR data and non-equilibrium nanosecond-simulations.

A major role for water in defining the equilibrium ensemble of GlcNAc puckers is proposed. Conformational exchange kinetics may therefore be difficult to predict without detailed and extended simulations. We re-iterate that for carbohydrates, longer empirical aqueous simulations are preferable to higher-level computation on short timescales and without water. Recent progress in computer hardware and software is enabling this for many carbohydrates without the need for artificial perturbation of systemic physical properties, as in enhanced sampling.

Substitution of the GlcNAc chemical scaffold did not affect rotamer preferences but did impact equilibrium ring puckering conformer populations and kinetics. Methylglycosides (a model for the glycosidic linkage) had slowed exchange kinetics due to reduced accessibility of biologically important skew boat intermediates. Sulfonation shifted the ensemble of puckers toward $^4C_1$, likely due to electrostatic repulsion and favorable solvation of equatorial sulfo groups.

Our 3D-structural and kinetic insights have extensive ramifications for understanding and exploiting 3D SARs in glycobiology. The importance of puckering in a myriad of GlcNAc-containing sugars (e.g. glycosaminoglycans, nodulation factors and glycosylation fragments) can now be tested experimentally. This iterative interdisciplinary approach, identification of pivotal kinetic 3D intermediates and concomitant-directed chemical modification of equilibrium conformer populations and exchange kinetics, has great potential to revolutionize glycan design.

Materials and methods

MD simulations

The monosaccharides were prepared using the AMBER tool Leap (Case et al. 2005) and in-house software (to define $^4C_1$ and $^1C_4$ puckers). Each of the 10 initial configurations was explicitly solvated in a cubic water box (~25 × 25 × 25 Å) and neutralized with the appropriate number of Na^+ counterions, followed by 1000 steps of energy minimization. MDs were performed with ACEMD (Harvey et al. 2009) on NVIDIA graphics processors using the force-fields GLYCAM06g (Kirschner et al. 2008) and TIP3P (Jorgensen et al. 1983). Hydrogen atoms were constrained using the M-SHAKE algorithm (Krautler et al. 2001). The velocity-Verlet integration algorithm and a hydrogen mass repartitioning scheme were used to achieve a 4 fs time-step without affecting the equilibrium distribution (Buch et al. 2010). Electrostatic and van der Waals interactions were truncated at 9 Å and the recommended scaling factor for carbohydrate 1–4 interactions (1.0) was used. Parameters not present in GLYCAM06 (the angle O-S-O and the torsion C2-O2-S-O) were appended from the General Amber Force-field (Wang et al. 2004). Merz–Singh–Kollman (Singh and Kollman 1984) electrostatic potential-derived partial charges for the sulfonated monosaccharides were computed using Gaussian 03 (Frisch et al. 2004) following gas-phase

geometry optimization at the HF/6-31G(d)//HF/6-31G(d) level of theory (consistent with GLYCAM06). Following 20 ns of heating and 250 ns of thermal equilibration at 298 K (which were discarded), MD simulations of each monosaccharide were performed for 10 μs in the NVT ensemble. Data were saved to file every 10 ps.

NMR spectroscopy

Natural abundance samples were prepared from lyophilized material (Dextra, Reading, UK) reconstituted in 594 μL of D_2O, 99.990% (w/v) and 6 μL of DSS (4,4-dimethyl-4-silapentane-1-sulfonic acid). Samples were adjusted to pD = 7.0 and final concentrations were in the range 41–56 mM. All spectra were recorded at 25°C. Chemical shifts of ^{1}H and ^{13}C atoms were assigned from the following standard heteronuclear NMR spectra recorded with a ^{1}H frequency of 600 MHz on a Bruker spectrometer equipped with a z-gradient TXI cryoprobe: [^{1}H–^{13}C] HSQC, [^{1}H–^{1}H] COSY, [^{1}H–^{1}H] TOCSY and a [^{1}H–^{13}C] HSQC–TOCSY. [^{1}H] 1D spectra were also recorded with a ^{1}H frequency of 900 MHz (Varian INOVA 900), 32,768 points, an acquisition time of 2949.17 ms and a dwell time of 45.5 μs. Vicinal couplings were measured from 900 MHz [^{1}H] 1D spectra unless otherwise stated. Spectra were processed with NMRPipe (Delaglio et al. 1995) and analyzed with Sparky (Goddard and Kneller 2006) and Analysis (Vranken et al. 2005). Proton chemical shifts were referenced relative to internal DSS and heteronuclei were referenced indirectly. As detailed previously (Blundell et al. 2004; Blundell, Deangelis, et al. 2006; Blundell, Reed, et al. 2006), appropriate linear prediction, window functions and zero-filling were used to achieve the maximum possible resolution from each data set.

QM calculations

Conformers representative of the complete pyranose Cremer–Pople (Cremer and Pople 1975) conformational space (74 in total) were built using in-house software, which systematically increments θ- and φ-parameters (by 30°) and then performs constrained gas-phase energy minimization (to maintain the pucker) using the UFF force field (Rappe et al. 1992). Single-point energy density functional theory calculations were performed on each geometry optimized conformer using Gaussian 03 (Frisch et al. 2004) at the B3LYP/6-311++G(*d*,*p*) level of theory in the gas phase and using the self-consistent reaction field polarizable continuum model (Cances et al. 1997; Cossi et al. 2002), whereby the electrostatic shielding effect of bulk solvent is treated as a continuous medium. The dielectric constant was set to 78.38, representative of water at 298.15 K. Charge and multiplicity values of 0/1, −1/1, −2/1 and −3/1 were used for GlcNAc and the mono-, di- and tri-sulfonated hexosamines, respectively.

Computed vicinal couplings and rotamer populations

Vicinal couplings were calculated using torsional data from the full 20 μs simulations for GlcNAc and 1-OMe-GlcNAc and from the 10 μs $^{4}C_1$-initiated trajectories for all other molecules. The sulfate-adjusted Karplus equation of Hricovini and Bizik (Altona and Haasnoot 1980; Hricovini and Bizik 2007) was used for ring vicinal couplings. The relationships of Altona and Haasnoot (1980) and Mobli and Almond (2007) were used for hydroxymethyl and acetamido (HN-N2-C2-H2) vicinal couplings, respectively. Values and standard deviations were obtained by computing the vicinal coupling for each 1 μs sub-trajectory and averaging. Hydroxyl orientations were binned as gauche(−), anti(*t*) or gauche(+) centered on −60, 180 and 60°, respectively. Hydroxymethyl conformations (*tg*, *gt* and *gg*) were defined by the torsions O6-C6-C5-O5 and O6-C6-C5-C4. To estimate hydroxymethyl rotamer populations directly from NMR data, the scalar couplings H5 to H6proR/S were fitted to a rigid three-site model (Poppe 1993) comprising variable populations of *tg*, *gt* and *gg* conformers using the relationships of Altona and Haasnoot.

Cremer–Pople analysis

Puckers were classified (using the pyranose ring atoms O5, C1, C2, C3, C4 and C5) by analysis of the Cremer–Pople (Cremer and Pople 1975) parameters Q, θ and φ, which are the radius, azimuthal and meridian angles (respectively) of the spherical puckering coordinate system describing all possible puckers for a six-membered ring. The Q-value represents the puckering magnitude (deviation from a flat ring), θ describes the type of pucker (chair, half-chair, boat, etc.) and φ is a phase angle describing pseudorotation. In the text and Supplementary data, a value of $\theta = 0°$ corresponds to $^{4}C_1$ and $\theta = 180°$ to $^{1}C_4$. Plots of each parameter, for each simulation, are reported in the Supplementary data S1. Equilibration of the simulations was assessed by comparing the convergence of the Cremer–Pople polar angle ácosθñ (which represents the average ring pucker, see Supplementary data S1), for simulations started in $^{4}C_1$ and $^{1}C_4$ puckers, as described previously (Sattelle et al. 2010). For analysis of GlcNAc 3D structures from the PDB, 794 and 13 GlcNAc and GlcNS6S crystallographic depositions were identified with resolution ≤2.0 Å, containing, respectively, 3137 and 16 3D structures. Acceptable limits of Q were defined as 0.8 (maximum) and 0.4 (minimum).

Free energy and rate constant and calculations

Free energies were derived from the relationship $\Delta G = |RT \ln (p1/p2)|$, where $p1$ and $p2$ are the equilibrium populations of $^{4}C_1$ and $^{1}C_4$ conformers, respectively, R the gas constant and T the temperature. Conformational exchange rates (k_1 and k_2) were derived by calculating the average time for transitions ($^{4}C_1 \rightarrow {}^{1}C_4$ and $^{1}C_4 \rightarrow {}^{4}C_1$) and taking the reciprocal. The reported equilibrium constants are the ratio of the rates, $K_{eq} = k_1/k_2$. The relationship $G = |RT \ln K_{eq}|$ was used to confirm computed free energies. These equations can be found in standard chemistry textbooks.

Supplementary data

Supplementary data for this article is available online at http://glycob.oxfordjournals.org/. Simulation data (S1 and S2), chemical shifts from NMR (S3) and 3D coordinates of the equilibrium GlcNAc conformer in water (S4) are provided.

Funding

This work was supported by the BBSRC UK (grant number BBG006768).

Acknowledgements

We gratefully acknowledge Dr. Sara Whittaker for useful discussions and also the University of Birmingham UK (Henry Welcome Building) for use of their 900 MHz NMR spectrometer.

Conflict of interest

None declared.

Abbreviations

CSD, Cambridge Structural Database; COSY, correlation spectroscopy; 3D, three-dimension; DSS, 4,4-dimethyl-4-silapentane-1-sulfonic acid; GlcA, β-D-glucuronic acid; GlcNAc, *N*-acetyl-D-glucosamine; HS, heparan sulfate; HSQC, heteronuclear single quantum coherence; IdoA, α-L-iduronic acid; IdoA2S, IdoA *2*-sulfate; MD, molecular dynamics; Me, methyl; NMR, nuclear magnetic resonance; 1-OMe, α-1-*O*-methylglycosides; PDB, Protein Data Bank; QM, quantum mechanics; SAR, structure–activity relationship; TOCSY, total correlation spectroscopy.

References

Altona C, Haasnoot CAG. 1980. Prediction of *anti* and *gauche* vicinal proton-proton coupling constants in carbohydrates: A simple additivity rule for pyranose rings. *Org Magn Reson*. 13:417–429.

Appell M, Strati G, Willett JL, Momany FA. 2004. B3LYP/6-311++G** study of α- and β-D-glucopyranose and 1,5-anhydro-D-glucitol: $^{4}C_{1}$ and $^{1}C_{4}$ chairs, $^{3,O}B$ and $B_{3,O}$ boats, and skew-boat conformations. *Carbohydr Res*. 339:537–551.

Ardevol A, Biarnes X, Planas A, Rovira C. 2010. The conformational free-energy landscape of β-D-mannopyranose: Evidence for a $^{1}S_{5} \rightarrow B_{2,5} \rightarrow {}^{O}S_{2}$ catalytic itinerary in β-mannosidases. *J Am Chem Soc*. 132:16058–16065.

Avci FY, Karst NA, Linhardt RJ. 2003. Synthetic oligosaccharides as heparin-mimetics displaying anticoagulant properties. *Curr Pharm Des*. 9:2323–2335.

Barnett CB, Naidoo KJ. 2010. Ring puckering: A metric for evaluating the accuracy of AM1, PM3, PM3CARB-1, and SCC-DFTB carbohydrate QM/MM simulations. *J Phys Chem B*. 114:17142–17154.

Barnett CB, Wilkinson KA, Naidoo KJ. 2010. Pyranose ring transition state is derived from cellobiohydrolase I induced conformational stability and glycosidic bond polarization. *J Am Chem Soc*. 132:12800–12803.

Barrows SE, Dulles FJ, Cramer CJ, French AD, Truhlar DG. 1995. Relative stability of alternative chair forms and hydroxymethyl conformations of β-D-glucopyranose. *Carbohydr Res*. 276:219–251.

Bishop JR, Schuksz M, Esko JD. 2007. Heparan sulphate proteoglycans fine-tune mammalian physiology. *Nature*. 446:1030–1037.

Blundell CD, Deangelis PL, Almond A. 2006. Hyaluronan: The absence of amide-carboxylate hydrogen bonds and the chain conformation in aqueous solution are incompatible with stable secondary and tertiary structure models. *Biochem J*. 396:487–498.

Blundell CD, DeAngelis PL, Day AJ, Almond A. 2004. Use of ^{15}N-NMR to resolve molecular details in isotopically-enriched carbohydrates: Sequence-specific observations in hyaluronan oligomers up to decasaccharides. *Glycobiology*. 14:999–1009.

Blundell CD, Reed MA, Overduin M, Almond A. 2006. NMR spectra of oligosaccharides at ultra-high field (900 MHz) have better resolution than expected due to favourable molecular tumbling. *Carbohydr Res*. 341:1985–1991.

Blundell CD, Roberts IS, Sheehan JK, Almond A. 2009. Investigating the molecular basis for the virulence of *Escherichia coli* K5 by nuclear magnetic resonance analysis of the capsule polysaccharide. *J Mol Microbiol Biotechnol*. 17:71–82.

Boltje TJ, Buskas T, Boons GJ. 2009. Opportunities and challenges in synthetic oligosaccharide and glycoconjugate research. *Nat Chem*. 1:611–622.

Buch I, Harvey MJ, Giorgino T, Anderson DP, De Fabritiis G. 2010. High-throughput all-atom molecular dynamics simulations using distributed computing. *J Chem Inf Model*. 50:397–403.

Cances E, Mennucci B, Tomasi J. 1997. A new integral equation formalism for the polarizable continuum model: Theoretical background and applications to isotropic and anisotropic dielectrics. *J Chem Phys*. 107:3032–3041.

Case DA, Cheatham TE, 3rd, Darden T, Gohlke H, Luo R, Merz KM, Jr., Onufriev A, Simmerling C, Wang B, Woods RJ. 2005. The Amber biomolecular simulation programs. *J Comput Chem*. 26:1668–1688.

Chang C, Magracheva E, Kozlov S, Fong S, Tobin G, Kotenko S, Wlodawer A, Zdanov A. 2003. Crystal structure of interleukin-19 defines a new subfamily of helical cytokines. *J Biol Chem*. 278:3308–3313.

Cossi M, Scalmani G, Rega N, Barone V. 2002. New developments in the polarizable continuum model for quantum mechanical and classical calculations on molecules in solution. *J Chem Phys*. 117:43–54.

Cremer D, Pople JA. 1975. General definition of ring puckering coordinates. *J Am Chem Soc*. 97:1354–1358.

Das SK, Mallet JM, Esnault J, Driguez PA, Duchaussoy P, Sizun P, Herault JP, Herbert JM, Petitou M, Sinay P. 2001. Synthesis of conformationally locked L-iduronic acid derivatives: Direct evidence for a critical role of the skew-boat $^{2}S_{0}$ conformer in the activation of antithrombin by heparin. *Chemistry*. 7:4821–4834.

Delaglio F, Grzesiek S, Vuister GW, Zhu G, Pfeifer J, Bax A. 1995. NMRPipe: A multidimensional spectral processing system based on UNIX pipes. *J Biomol NMR*. 6:277–293.

Dowd MK, French AD, Reilly PJ. 1994. Modeling of aldopyranosyl ring puckering with MM3(92). *Carbohydr Res*. 264:1–19.

Frisch MJ, Trucks GW, Schlegel HB, Scuseria GE, Robb MA, Cheeseman JR, Montgomery JJA, Vreven T, Kudin KN, Burant JC, et al. 2004. *Gaussian 03, Revision C.02*.

Gama CI, Tully SE, Sotogaku N, Clark PM, Rawat M, Vaidehi N, Goddard WA, 3rd, Nishi A, Hsieh-Wilson LC. 2006. Sulfation patterns of glycosaminoglycans encode molecular recognition and activity. *Nat Chem Biol*. 2:467–473.

Gao YQ, Yang LJ, Fan YB, Shao Q. 2008. Thermodynamics and kinetics simulations of multi-time-scale processes for complex systems. *Int Rev Phys Chem*. 27:201–227.

Ghosh T, Chattopadhyay K, Marschall M, Karmakar P, Mandal P, Ray B. 2009. Focus on antivirally active sulfated polysaccharides: From structure-activity analysis to clinical evaluation. *Glycobiology*. 19:2–15.

Goddard TD, Kneller DG. 2006. *SPARKY 3*. San Francisco: University of California.

Harvey MJ, Giupponi G, De Fabritiis G. 2009. ACEMD: Accelerating biomolecular dynamics in the microsecond time scale. *J Chem Theory Comput*. 5:1632–1639.

Heymann B, Grubmuller H. 1999. 'Chair-boat' transitions and side groups affect the stiffness of polysaccharides. *Chem Phys Lett*. 305:202–208.

Hricovini M, Bizik F. 2007. Relationship between structure and three-bond proton-proton coupling constants in glycosaminoglycans. *Carbohydr Res*. 342:779–783.

Hricovini M, Guerrini M, Bisio A, Torri G, Petitou M, Casu B. 2001. Conformation of heparin pentasaccharide bound to antithrombin III. *Biochem J*. 359:265–272.

Ikemizu S, Sparks LM, van der Merwe PA, Harlos K, Stuart DI, Jones EY, Davis SJ. 1999. Crystal structure of the CD2-binding domain of CD58 (lymphocyte function-associated antigen 3) at 1.8-A resolution. *Proc Natl Acad Sci USA*. 96:4289–4294.

Jefferis R. 2009. Glycosylation as a strategy to improve antibody-based therapeutics. *Nat Rev Drug Discovery*. 8:226–234.

Jin L, Hricovini M, Deakin JA, Lyon M, Uhrin D. 2009. Residual dipolar coupling investigation of a heparin tetrasaccharide confirms the limited effect of flexibility of the iduronic acid on the molecular shape of heparin. *Glycobiology*. 19:1185–1196.

Johnson LN. 1966. The crystal structure of *N*-acetyl-α-D-glucosamine. *Acta Crystallogr*. 21:885–891.

Jorgensen WL, Chandrasekhar J, Madura JD, Impey RW, Klein ML. 1983. Comparison of simple potential functions for simulating liquid water. *J Chem Phys*. 79:926–935.

Khoushab F, Yamabhai M. 2010. Chitin research revisited. *Mar Drugs*. 8:1988–2012.

Kirschner KN, Woods RJ. 2001. Solvent interactions determine carbohydrate conformation. *Proc Natl Acad Sci USA*. 98:10541–10545.

Kirschner KN, Yongye AB, Tschampel SM, Gonzalez-Outeirino J, Daniels CR, Foley BL, Woods RJ. 2008. GLYCAM06: A generalizable biomolecular force field. Carbohydrates. *J Comput Chem*. 29:622–655.

Klepeis JL, Lindorff-Larsen K, Dror RO, Shaw DE. 2009. Long-timescale molecular dynamics simulations of protein structure and function. *Curr Opin Struct Biol*. 19:120–127.

Krautler V, Van Gunsteren WF, Hunenberger PH. 2001. A fast SHAKE: Algorithm to solve distance constraint equations for small molecules in molecular dynamics simulations. *J Comput Chem*. 22:501–508.

Lamanna WC, Kalus I, Padva M, Baldwin RJ, Merry CLR, Dierks T. 2007. The heparanome—The enigma of encoding and decoding heparan sulfate sulfation. *J Biotechnol*. 129:290–307.

Li HB, Rief M, Oesterhelt F, Gaub HE, Zhang X, Shen JC. 1999. Single-molecule force spectroscopy on polysaccharides by AFM – nanomechanical fingerprint of α-(1,4)-linked polysaccharides. *Chem Phys Lett*. 305:197–201.

Liu J, Pedersen LC. 2007. Anticoagulant heparan sulfate: Structural specificity and biosynthesis. *Appl Microbiol Biotechnol*. 74:263–272.

Liu H, Zhang Z, Linhardt RJ. 2009. Lessons learned from the contamination of heparin. *Nat Prod Rep*. 26:313–321.

Marino K, Bones J, Kattla JJ, Rudd PM. 2010. A systematic approach to protein glycosylation analysis: A path through the maze. *Nat Chem Biol*. 6:713–723.

Marszalek PE, Oberhauser AF, Pang YP, Fernandez JM. 1998. Polysaccharide elasticity governed by chair-boat transitions of the glucopyranose ring. *Nature*. 396:661–664.

Maruyama T, Toida T, Imanari T, Yu GY, Linhardt RJ. 1998. Conformational changes and anticoagulant activity of chondroitin sulfate following its *O*-sulfonation. *Carbohydr Res*. 306:35–43.

Maveyraud L, Niwa H, Guillet V, Svergun DI, Konarev PV, Palmer RA, Peumans WJ, Rouge P, Van Damme EJA, Reynolds CD, et al. 2009. Structural basis for sugar recognition, including the Tn carcinoma antigen, by the lectin SNA-II from *Sambucus nigra*. *Proteins Struct Funct Bioinf*. 75:89–103.

Mo F, Jensen LH. 1975. Refined model for *N*-acetyl-α-D-glucosamine. *Acta Crystallogr Sect B: Struct Sci*. 31:2867–2873.

Mobli M, Almond A. 2007. *N*-Acetylated amino sugars: The dependence of NMR $^{3}J_{(HNH2)}$-couplings on conformation, dynamics and solvent. *Org Biomol Chem*. 5:2243–2251.

Mobli M, Nilsson M, Almond A. 2008. The structural plasticity of heparan sulfate NA-domains and hence their role in mediating multivalent interactions is confirmed by high-accuracy ^{15}N-NMR relaxation studies. *Glycoconj J*. 25:401–414.

Morando MA, Nurisso A, Grenouillat N, Vauzeilles B, Beau JM, Canada FJ, Jimenez-Barbero J, Imberty A. 2011. NMR and molecular modeling reveal key structural features of synthetic nodulation factors. *Glycobiology*. 21:824–833.

Mulloy B, Forster MJ. 2000. Conformation and dynamics of heparin and heparan sulfate. *Glycobiology*. 10:1147–1156.

Mulloy B, Johnson EA. 1987. Assignment of the ^{1}H-n.m.r. spectra of heparin and heparan sulphate. *Carbohydr Res*. 170:151–165.

Murrey HE, Hsieh-Wilson LC. 2008. The chemical neurobiology of carbohydrates. *Chem Rev*. 108:1708–1731.

Nishiyama Y, Noishiki Y, Wada M. 2011. X-ray structure of anhydrous β-chitin at 1 angstrom resolution. *Macromolecules*. 44:950–957.

Nothaft H, Szymanski CM. 2010. Protein glycosylation in bacteria: Sweeter than ever. *Nat Rev Microbiol*. 8:765–778.

Ojala WH, Albers KE, Gleason WB, Choo CG. 1995. Carbohydrates with relevance to the structure of glycosaminoglycans: The crystal-structures of 2-deoxy-2-(sulfoamino)-α-D-glucopyranose sodium salt dihydrate, 2-amino-2-deoxy-α,β-D-glucopyranose 3-(hydrogen sulfate) monohydrate, and 2-amino-2-deoxy-α-D-glucopyranose 6-(hydrogen sulfate) monohydrate. *Carbohydr Res*. 275:49–65.

Orozco M, Noy A, Perez A. 2008. Recent advances in the study of nucleic acid flexibility by molecular dynamics. *Curr Opin Struct Biol*. 18:185–193.

Poppe L. 1993. Modeling carbohydrate conformations from NMR data: Maximum-entropy rotameric distribution about the C5-C6 bond in gentiobiose. *J Am Chem Soc*. 115:8421–8426.

Powell AK, Yates EA, Fernig DG, Turnbull JE. 2004. Interactions of heparin/heparan sulfate with proteins: Appraisal of structural factors and experimental approaches. *Glycobiology*. 14:17R–30R.

Rabenstein DL. 2002. Heparin and heparan sulfate: Structure and function. *Nat Prod Rep*. 19:312–331.

Rappe AK, Casewit CJ, Colwell KS, Goddard WA, Skiff WM. 1992. Uff, a full periodic-table force-field for molecular mechanics and molecular-dynamics simulations. *J Am Chem Soc*. 114:10024–10035.

Rich A. 2003. The double helix: A tale of two puckers. *Nat Struct Biol*. 10:247–249.

Sasisekharan R, Shriver Z, Venkataraman G, Narayanasami U. 2002. Roles of heparan-sulphate glycosaminoglycans in cancer. *Nat Rev Cancer*. 2:521–528.

Sattelle BM, Almond A. 2010. Less is more when simulating unsulfated glycosaminoglycan 3D-structure: Comparison of GLYCAM06/TIP3P, PM3-CARB1/TIP3P, and SCC-DFTB-D/TIP3P predictions with experiment. *J Comput Chem*. 31:2932–2947.

Sattelle BM, Hansen SU, Gardiner J, Almond A. 2010. Free energy landscapes of iduronic acid and related monosaccharides. *J Am Chem Soc*. 132:13132–13134.

Schlick T. 2009. Molecular dynamics-based approaches for enhanced sampling of long-time, large-scale conformational changes in biomolecules. *F1000 Biol Rep*. 1:51.

Singh UC, Kollman PA. 1984. An approach to computing electrostatic charges for molecules. *J Comput Chem*. 5:129–145.

Smits NC, Kurup S, Rops AL, ten Dam GB, Massuger LF, Hafmans T, Turnbull JE, Spillmann D, Li JP, Kennel SJ, et al. 2010. The heparan sulfate motif $(GlcNS6S\text{-}IdoA2S)_3$, common in heparin, has a strict topography and is involved in cell behavior and disease. *J Biol Chem*. 285:41143–41151.

Spiwok V, Kralova B, Tvaroska I. 2010. Modelling of β-D-glucopyranose ring distortion in different force fields: A metadynamics study. *Carbohydr Res*. 345:530–537.

Toida T, Maruyama T, Ogita Y, Suzuki A, Toyoda H, Imanari T, Linhardt RJ. 1999. Preparation and anticoagulant activity of fully *O*-sulphonated glycosaminoglycans. *Int J Biol Macromol*. 26:233–241.

Toida T, Suzuki A, Nakajima K, Chaidedgumjorn A, Imanari T. 2000. Effect of 6-*O*-sulfonate hexosamine residue on anticoagulant activity of fully *O*-sulfonated glycosaminoglycans. *Glycoconj J*. 17:393–399.

Turnbull JE. 2010. Heparan sulfate glycomics: Towards systems biology strategies. *Biochem Soc Trans*. 38:1356–1360.

Vranken WF, Boucher W, Stevens TJ, Fogh RH, Pajon A, Llinas M, Ulrich EL, Markley JL, Ionides J, Laue ED. 2005. The CCPN data model for NMR spectroscopy: Development of a software pipeline. *Proteins*. 59:687–696.

Wang Z, Du J, Che PL, Meledeo MA, Yarema KJ. 2009. Hexosamine analogs: From metabolic glycoengineering to drug discovery. *Curr Opin Chem Biol*. 13:565–572.

Wang JM, Wolf RM, Caldwell JW, Kollman PA, Case DA. 2004. Development and testing of a general amber force field. *J Comput Chem*. 25:1157–1174.

Wessel HP, Bartsch S. 1995. Conformational flexibility in highly sulfated β-D-glucopyranoside derivatives. *Carbohydr Res*. 274:1–9.

Xu R, McBride R, Paulson JC, Basler CF, Wilson IA. 2010. Structure, receptor binding, and antigenicity of influenza virus hemagglutinins from the 1957 H2N2 pandemic. *J Virol*. 84:1715–1721.

Yates EA, Mackie W, Lamba D. 1995. The crystal and molecular-structure of 2-sulfamino-2-deoxy-α-D-glucopyranose sodium salt.$2H_2O$ (glucosamine 2-sulfate). *Int J Biol Macromol*. 17:219–226.

Zhu HL, Fernandez C, Fan JB, Shewmaker F, Chen J, Minton AP, Liang Y. 2010. Quantitative characterization of heparin binding to Tau protein: Implication for inducer-mediated Tau filament formation. *J Biol Chem*. 285:3592–3599.